JOURNAL OF PHYSICAL ORGANIC CHEMISTRY
J. Phys. Org. Chem. 2005; **18:** 602–609
Published online 11 February 2005 in Wiley InterScience (www.interscience.wiley.com). DOI: 10.1002/poc.906

Comparative analysis of NMR spectral parameters and molecular dynamics of 1:6-anhydro-3:4-thia-2-*O*-tosyl-β-D-allopyranose and 1,6:3,4-dianhydro-2-*O*-tosyl-β-D-galactopyranose in the solid phase

Marek J. Potrzebowski,[1]* Sławomir Kaźmierski,[1] Sebastian Olejniczak,[1] Jan Heliński,[1] Włodzimierz Ciesielski[1] and Andreas Dőlle[2]

[1]Polish Academy of Sciences, Center of Molecular and Macromolecular Studies, Sienkiewicza 112, 90-363 Łódź, Poland
[2]Institut für Physikalische Chemie, RWTH Aachen, Templergraben 59, 52056 Aachen, Germany

Received 23 August 2004; revised 3 December 2004; accepted 30 December 2004

ABSTRACT: A search of x-ray data for 1:6-anhydro-3:4-thia-2-*O*-tosyl-β-D-allopyranose (**1**) and 1:6,3:4-dianhydro-2-*O*-tosyl-β-D-galactopyranose (**2**) revealed two C—H···O intermolecular contacts for both compounds and one C—H···S interaction for **1**. Inspection of hydrogen bonding showed that these interactions are stronger for **2**. The ^{13}C relaxation times in the rotating frame, $^{13}C\ T^*_{1\rho}$, measured at $B_1 = 36.7$ kHz showed apparent differences in internal molecular motion on the kilohertz scale for both samples. A PASS-2D experiment recorded at a spinning rate of 1 kHz was performed to establish the values of principal elements of chemical shift tensors $^{13}C\ \delta_{ii}$. DFT GIAO calculations of shielding parameters were carried out and the orientations of $^{13}C\ \delta_{ii}$ were assigned. An attempt to correlate ^{13}C NMR spectral parameters and molecular dynamics in the solid state with structure, internal motion and intermolecular interactions is presented. Copyright © 2005 John Wiley & Sons, Ltd.
Supplementary electronic material for this paper is available in Wiley Interscience at http://www.interscience.wiley.com/jpages/0894-3230/suppmat/

KEYWORDS: C—H···O, C—H···S intermolecular contacts; ^{13}C relaxation time; rotating frame; DFT GIAO calculations; molecular motion; solid-state NMR

INTRODUCTION

Carbohydrates are one of the most important components of living organisms and attractive models for structural studies.[1,2] The richness of possible structural modifications raises questions regarding the relationship between the structure and biological functions. Several experimental techniques have been used to assign the structures and dynamic properties of natural products, but NMR spectroscopy is one of the most valuable.[3–5] Applications of this method in structural studies of carbohydrates in solution[6–8] but much less in the solid state[9] have been reported.

Anhydro sugars have received much attention as versatile intermediates in carbohydrate syntheses, giving access to sugar amino acids and peptides, branched-chain, cyclopropanated and aziridino sugars and other derivatives.[10] Their thio analogs are attractive synthons often used in stereospecific syntheses of natural products.[11] In this paper, we present NMR studies of two sugar derivatives that belong to class of compounds mentioned above: 1:6-anhydro-3:4-thia-2-*O*-tosyl-β-D-allopyranose (**1**) and 1:6,3:4-dianhydro-2-*O*-tosyl-β-D-galactopyranose (**2**). Both molecules are very rigid owing to presence of three- and five-membered rings. Such entities offer several possibilities for use as models to

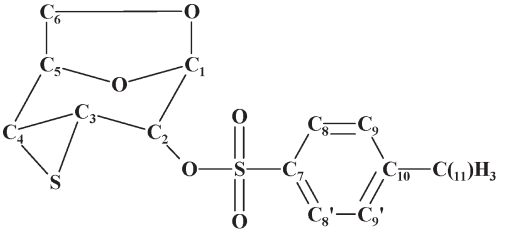

1

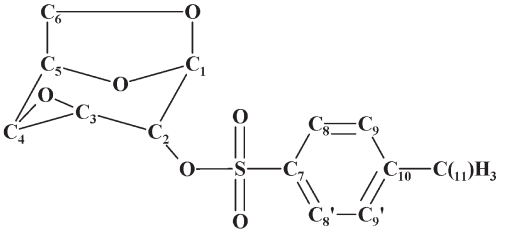

2

**Correspondence to:* M. J. Potrzebowski, Polish Academy of Sciences, Center of Molecular and Macromolecular Studies, Sienkiewicza 112, 90-363 Łódź, Poland.
E-mail: marekpot@bilbo.cbmm.lodz.pl

test the relationship between structure, molecular dynamics and spectral parameters. The 1,6-anhydro derivatives of monosaccharides are found to be convenient species to study overall motion since the presence of the five-membered anhydro ring precludes changes of conformation of the sugar residue. Rigid carbohydrates usually reorient anisotropically in the liquid phase and can be employed to test the different theoretical approaches used in calculations of fully asymmetric motion.[12,13] Compounds containing three-membered rings have recently attracted attention as models for theoretical calculations of NMR parameters. Krivdin *et al.* have reported non-empirical calculations of indirect carbon–carbon coupling constants in different hetero-organic derivatives of cyclopropane.[14]

In this work, we were attracted by the prospect of checking whether molecules **1** and **2** are rigid in the crystal lattice or undergo any kind of molecular motion. We present comparative NMR studies of spectral parameters. Experimental and theoretical values of ^{13}C NMR shielding for **1** and **2** are used to establish the influence of replacing of oxygen by sulfur in the three-membered ring. ^{13}C $T_{1\rho}$ relaxation times were measured in order to correlate molecular dynamics with weak intermolecular interactions, e.g. C—H···O hydrogen bonds.

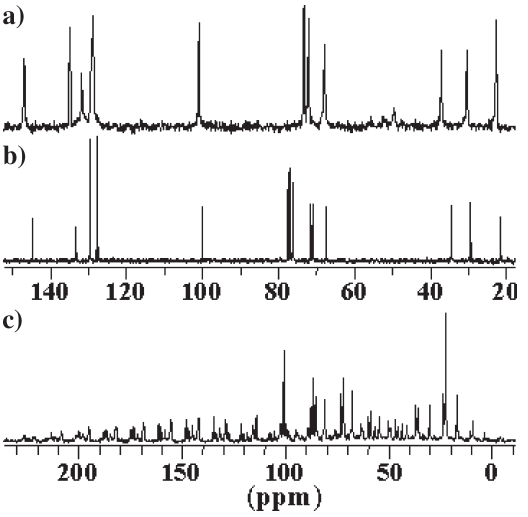

Figure 1. (a) 75.46 MHz ^{1}H–^{13}C CP/MAS experimental spectrum of **1** recorded with spinning rate 7 kHz; (b) ^{13}C NMR spectrum recorded in solution (chloroform-*d*); (c) CP/MAS spectrum recorded with spinning rate 1 kHz

RESULTS

^{13}C solid-state NMR studies

The crystal and molecular structures of **1** and **2** in the solid state have been published.[15,16] Preliminary NMR studies for **2** have been reported elsewhere.[17,18] The ^{13}C cross-polarization magic angle spinning (CP/MAS) spectrum of **1** recorded at 7 kHz with RAMP shape cross-polarization[19] and TPPM decoupling[20] is shown in Fig. 1(a). The rough assignment of isotropic chemical shifts for **1** was done by data comparison with those obtained in the liquid phase [Fig. 1(b)]. ^{13}C δ_{iso} SS NMR data for **1** and **2** are given in Table 1.

From comparative analysis of chemical shift parameters, it is clear that the greatest differences are seen for C3 ($\Delta = -17.6$ ppm), C4 ($\Delta = -14.7$ ppm), methylene carbons C6 ($\Delta = 3.7$ ppm) and aromatic carbons C9′ ($\Delta = 8.0$ ppm). It is well known, however, that more information about the electronic surrounding of each nucleus, which reflects subtle structural effects, can be obtained from inspection of the tensorial nature of the chemical shift. Hence, in this part of the project we were attracted by the prospect of the analysis of ^{13}C δ_{ii} data for **1**, inspection of anisotropic values of chemical shift tensors and correlation of the principal elements to the molecular structure. For rotating solids, ^{13}C δ_{ii} parameters can be obtained from the analysis of spinning sideband intensities. For the sample under investigation, the spinning rate should be in range 2–3 kHz to obtain a spectrum with a sufficient number of sidebands for further calculations of the aromatic region. For aliphatic signals the spinning rate should be even smaller, in region of 1 kHz. As we found for **1**, deconvolution is not an easy task. At low spinning rate [Fig. 1(c)] the overlap between different spinning sideband manifolds and analysis of the spectrum is ambiguous.

The separation of isotropic and anisotropic parts of spectra with heavy overlapped systems is still a challenge for solid-state NMR spectroscopy. There are several approaches, that allow this goal to be achieved.[21] In our project, we employed the PASS 2D sequence, which compared with other techniques offers good sensitivity and does not require any hardware modifications or special probehead. A detailed explanation on the PASS-2D pulse sequence, its performance, a Mathematica routine to generate a set of PASS solutions and the data processing can be found elsewhere.[22,23] Figure 2(a)

Table 1. ^{13}C chemical shifts (ppm) for **1** and **2** in the solid state and the differences $\Delta = \delta_1 - \delta_2$ (ppm)

Compound	C1	C2	C3	C4	C5	C6	C7	C8	C8′	C9	C9′	C10	C11
1	100.0	73.4	30.3	37.1	72.2	68.0	135.1	135.3	129.3	127.0	137.1	147.1	22.7
2	98.1	71.9	47.6	51.8	71.2	64.3	133.1	133.1	131.1	127.6	129.1	147.8	23.2
Δ	1.9	1.5	−17.6	−14.7	1.0	3.7	2.0	2.0	−1.8	−0.6	8.0	−0.7	−0.5

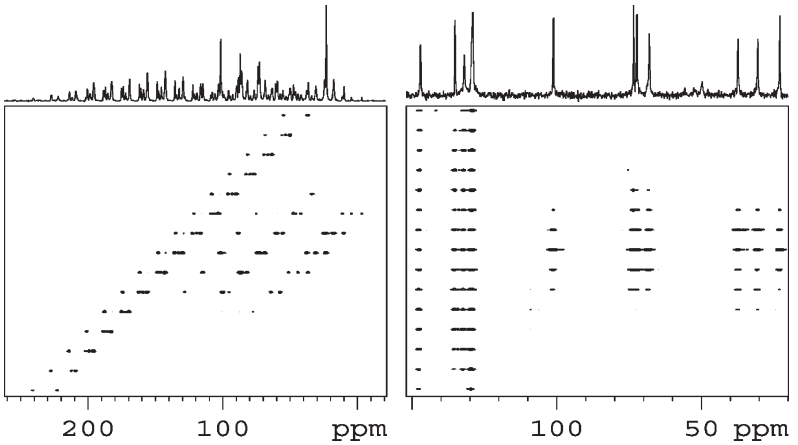

Figure 2. PASS-2D spectrum of **1** (a) recorded with spinning rate 1 kHz and (b) after proper data shearing

displays the PASS-2D spectrum of **1**, recorded with a spinning rate of 1 kHz.

The aromatic atoms are characterized by a large CSA and under slow sample spinning the spectrum presents a complex pattern. By tilting the spectrum in Fig. 2(a) it is possible to separate the spinning sidebands for each carbon [Fig. 2(b)] and, employing a calculation procedure, establish the ^{13}C δ_{ii} parameters. It is clear from such a presentation that the F_2 projection corresponds to TOSS[24] spectrum whereas the F_1 projection represents CSA. In this work, ^{13}C δ_{ii} values were obtained by means of the SIMPSON program.[25] A similar procedure was employed for the analysis of ^{13}C CST parameters of **2**. The experimental and the best-fitting simulated 1D spinning CSA sideband patterns for **1** and **2** are shown in Fig. 3. The ^{13}C δ_{ii} parameters are given in Table 2.

GIAO calculations of ^{13}C NMR parameters

A number of methods are currently available for computing of NMR parameters.[26,27] In our work, the GIAO B3PW91 hybrid method and 6–311++G** basis set was used for calculation of the ^{13}C parameters of **1** employing the Gaussian program.[28] The x-ray diffraction data of **1** were taken as an input file.[15] The advantage of such an approach is related to the fact that it is possible to compare the theoretical and experimental results for molecules with exactly the same geometry of heavy atoms. The position of hydrogen atoms has to be optimized since x-ray diffraction often has difficulty in locating protons accurately. How important C—H bond length optimization is in GIAO computing of ^{13}C NMR parameters has been discussed elsewhere.[29] The theoretical ^{13}C chemical shielding parameters calculated by means of the GIAO method for **1** are given in Table 3.

Figure 4 shows the correlation of the experimental chemical shift δ_{ii} parameters with the shielding parameters. The equation $\delta_{ii} = 176.06 - 0.908\sigma_{ii}$ ($R^2 = 0.9894$) can be employed to convert shielding to chemical shift parameters. The data obtained provide unambiguous evidence confirming the correctness of the GIAO calculations. The values of the calculated ^{13}C δ_{ii} parameters for sugar carbons of **1** are in range of those established for **2**.[18] Comparing the reference data, the greatest differences are found for carbons C3 and C4. For these carbons, the δ_{ii} for **1** are regularly upfield by ca 20 ppm compared with **2**.

The advantage of the theoretical approach is that in contrast to the CP/MAS experiment, not only values but also the orientation of the principal elements of chemical shift tensors can be obtained. Figure 5(a) shows the orientation of ^{13}C δ_{ii} parameters with respect to the molecular frame of **1**. In principle, the δ_{33} elements

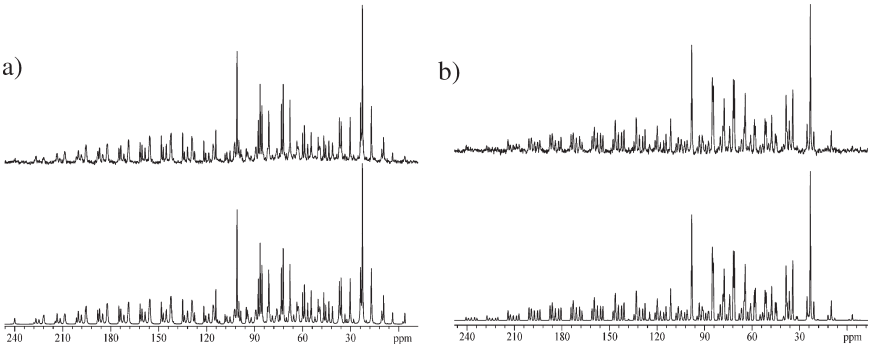

Figure 3. Experimental and the best-fitting simulated 1D spinning CSA sideband pattern for (a) **1** and (b) **2** with values obtained from the PASS-2D experiment. Experimental spectra recorded with spinning rate 1 kHz are shown as top traces

Table 2. ^{13}C chemical shift parameters for **1** and **2** obtained by analysis of PASS-2D spectra

Compound	Carbon	δ_{iso} (ppm)	δ_{11} (ppm)	δ_{22} (ppm)	δ_{33} (ppm)	Span Ω (ppm)	Skew κ
1	1	100.0	126	98	79	47	−0.13
	2	73.4	102	87	30	72	0.57
	3	30.3	70	16	4	66	−0.65
	4	37.1	77	25	9	68	−0.53
	5	72.2	100	78	39	61	0.28
	6	68.0	97	74	33	64	0.28
	7	135.1	207	144	54	153	0.17
	8	129.3	214	151	22	192	0.34
	8′	125.3	216	149	21	195	0.36
	9	137.1	221	145	30	181	0.13
	9′	127.0	215	140	33	182	0.21
	10	147.1	231	174	37	194	0.47
	11	22.7	37	31	0	37	0.67
2	1	98.1	122	96	76	46	−0.14
	2	71.9	97	81	38	59	0.46
	3	47.6	95	27	21	74	−0.84
	4	51.8	103	36	16	87	−0.54
	5	71.2	97	79	37	60	0.39
	6	64.3	90	74	29	61	0.48
	7	133.1	214	142	43	171	0.16
	8	133.1	214	143	43	171	0.17
	8′	131.1	218	153	22	196	0.36
	9	127.6	220	136	26	194	0.13
	9′	129.1	216	153	19	197	0.36
	10	147.8	234	181	28	206	0.48
	11	23.2	37	29	5	32	0.54

Estimated errors in δ_{11}, δ_{22} and δ_{33} are ± 3 ppm; span is expressed as $\Omega = \delta_{11} - \delta_{33}$, skew as $\kappa = 3\ (\delta_{22} - \delta_{iso})/\Omega$.

Table 3. Values of calculated ^{13}C chemical shielding parameters σ_{ii} for **1**[a]

Carbon	σ_{11} (ppm)	σ_{22} (ppm)	σ_{33} (ppm)
1	60.4	85.8	100.3
2	81.4	93.0	151.4
3	106.8	163.1	179.0
4	96.2	166.4	179.0
5	92.5	107.8	148.2
6	86.1	110.0	154.1
7	−29.0	31.7	137.0
8	−39.9	28.2	178.7
8′	−35.8	36.1	178.5
9	−54.6	39.4	158.7
9′	−39.4	44.2	169.0
10	−77.8	16.5	175.3
11	142.4	160.0	197.4

[a] The equation $\delta_{ii} = -0.908\sigma_{ii} + 176.06$ can be used to convert shielding to chemical shift.

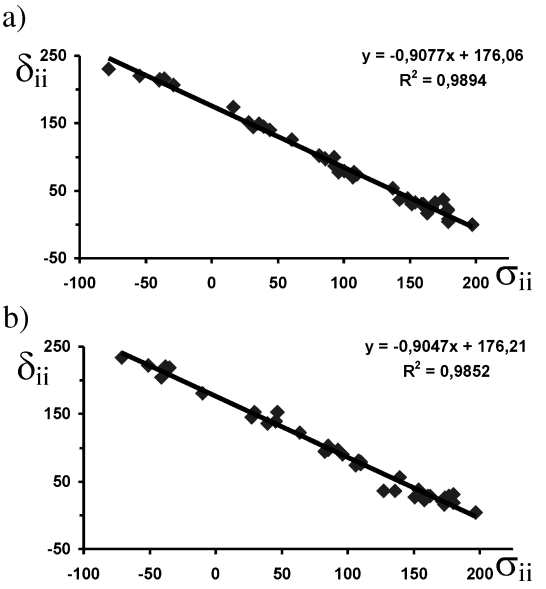

Figure 4. Correlation of the experimental versus calculated ^{13}C chemical shift δ_{ii} parameters and σ_{ii} shielding parameters for (a) **1** and (b) **2**. The shielding parameters for **2** are taken from Ref. 18

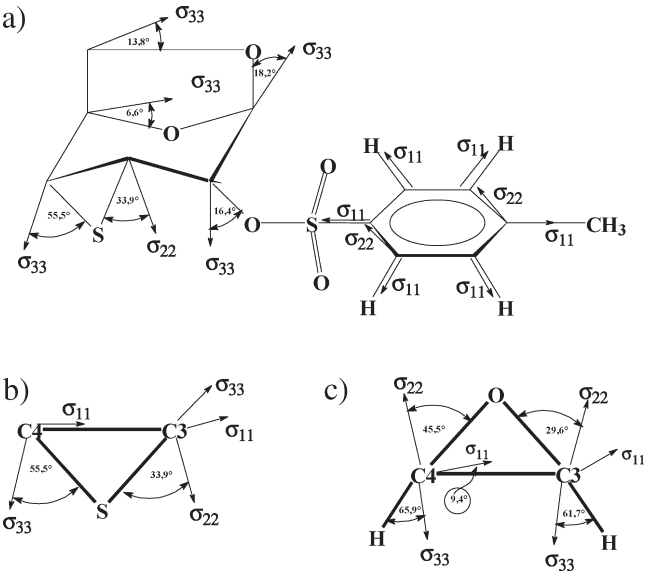

Figure 5. (a) Orientation of the principal elements of the chemical shift tensor with respect to the structure of **1**; (b) differences for C3—O—C4 fragments of **1** and **2**

are oriented along the C—O bonds whereas δ_{22} are aligned in the O—C—O plane. Such an alignment is consistent with data reported by Sastry *et al.* for methyl glycoside.[30] For **1**, the exceptions are the C3 and C4 carbons forming a three-membered ring. For C3, δ_{33} is perpendicular to the C4—C3—S plane [Fig. 5(b)]. For C4, δ_{33} deviates significantly from the C—S bond. It is interesting that δ_{11} of C4 is oriented along the C4—C3 bond. Comparison of this fragment of the molecule with the analogous part of **2** revealed significant differences in the orientation of ^{13}C δ_{ii} [Fig. 5(b)]. In the case of **2**, for both carbons the δ_{33} parameters are oriented along the C—H bond.

The theoretical ^{13}C δ_{ii} elements for the tosyl group were discussed in detail in a previous paper.[17] The values obtained in this work are roughly similar, hence the conclusion drawn before is also valid for **1**. It is worth noting that as in the case of other aromatic systems, the δ_{11} elements are aligned along C—H bonds, δ_{22} are in the

Table 4. Values of ^{13}C effective $T^*_{1\rho}$ relaxation times with $B_1 = 36.7$ kHz

Compound	C1	C2	C3	C4	C5	C6	C7	C8	C9	C10	C11
1	26.1	22.3	29.3	25.3	20.9	4.3	161.3	33.2	31.5	185.2	96.1
2	39.5	39.1	60.2	51.0	39.1	12.0	322.6	39.5	39.5	466.7	112.3

aromatic plane whereas δ_{33} are perpendicular to this plane. Moreover, replacing the hydrogen by a sulfonyl group (C7) does not change the orientation of δ_{11} and this element is placed along the C—S bond.

Analysis of dynamic properties of 1 and 2 in the solid state

Various relaxation parameters have utility for elucidating dynamics in the solid state, e.g. ^{13}C and ^{1}H spin–lattice relaxation times (^{13}C T_1 and ^{1}H T_1), carbon and proton rotating frame relaxation times (^{13}C $T_{1\rho}$ and ^{1}H $T_{1\rho}$), the C—H cross-relaxation time ($T_{C—H}$) and the proton relaxation time in the dipolar state (T_{1D}).[31] Not all of these parameters provide information in a direct manner; however, in the complementary approach one can establish the amplitudes and motional frequencies for solids in a broad range. For instance, the ^{13}C T_1 and ^{13}C $T_{1\rho}$ measurements provide information on molecular motions in the megahertz and kilohertz frequency ranges, respectively.

The ^{13}C T_1 data for **1** were recorded with the pulse sequence published by Torchia.[32] The results are consistent with those reported for **2**.[17] The relaxation times are very long (>200 s) for all carbon atoms with the exception of the methyl group, which undergoes fast reorientation; ^{13}C T_1 for CH_3 is found to be 55 s. More interesting information was found on searching the ^{13}C relaxation parameters in the rotating frame.[33,34] The measurements were carried out at five B_1 spin locking frequencies: 83.3, 57.9, 36.7, 34.0 and 27.8 kHz. At the highest B_1 frequency, decay of magnetization in the rotating frame was not observed for any carbon. At 57.9 kHz, minute differences in the rates decay of aromatic quaternary carbons and other aromatic and sugar carbons appeared. Significant differences in ^{13}C $T_{1\rho}$ were observed between carbons of **1** at $B_1 = 36.7$ kHz and other lower frequencies of spin locking. Inspection of Table 4 and Fig. 6 provides straightforward evidence for this.

The greatest distinction is seen for C6 carbon (^{13}C $T_{1\rho} = 4.3$ ms at 36.7 kHz) and other carbons (^{13}C $T_{1\rho} > 20$ ms). Although such results suggest large differences in the motional behavior of individual atoms, care must be taken in the interpretation of relaxation data in the rotating frame. The measured relaxation time is defined as the effective $T^*_{1\rho}$, where

$$(T^*_{1\rho})^{-1} = (T^C_{1\rho})^{-1} + (T^D_{C—H})^{-1} \quad (1)$$

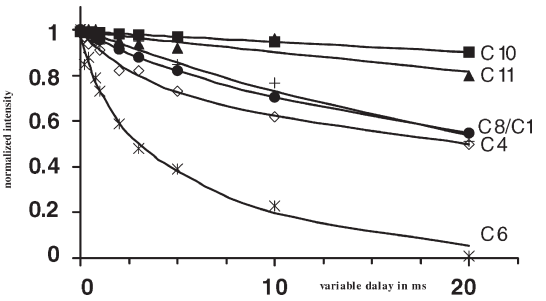

Figure 6. ^{13}C $T_{1\rho}$ for well-resolved carbons of **1** obtained at spin locking field $B_1 = 36.7$ kHz.

and further

$$(T^C_{1\rho})^{-1} = N_H\gamma_H^2\gamma_C^2h^2f(\tau_C)r_{C-H}^{-6}/20 \quad (2)$$

$$f(\tau_C) = [2J(\omega_1) + 0.5J(\omega_H - \omega_C) + 1.5J(\omega_C) + 3J(\omega_H) + 3J(\omega_H + \omega_C \quad (3)$$

$$J(\omega_i) = 2\tau_C/(1 + \omega_i^2\tau_C^2) \quad (4)$$

and

$$(T^D_{C-H})^{-1} = 0.5\sin^2\Theta M^{(2)}_{C-H}J_D(\omega_{1C}) \quad (5)$$

where $M^{(2)}_{C-H}$ is the second moment of the carbon nucleus from the dipolar interaction with protons, Θ is the off-resonance angle of the applied r.f. field and $J_D(\omega_{1C}) = \pi\tau_D\exp(-2\pi B_1\tau_D)$, where τ_D is the correlation time for spin fluctuation.

It is apparent from the above equations that two pathways of relaxation have different dependences of the applied rotating-frame field. When the correlation times are long compared with the inverse of Zeeman field Larmor frequencies, only the $J(\omega_1)$ term is important in Eqn (2). On the other hand, the contribution T^D_{C-H} in Eqn (5) has an exponential dependence on ω_1. This field dependence is one of the methods that allows a separation of the contributions to the effective $T^*_{1\rho}$. At $B_1 = 36.7$ kHz, the $T^*_{1\rho}$ data for CH carbons of the sugar ring display an exponential dependence on the rotating-frame field as predicted for the spin–spin (T^D_{C-H}) relaxation pathway. For C1—C4 carbons, ^{13}C $T^*_{1\rho}$ is in range 29–22 ms and for C5 is slightly shorter (20.9 ms). As already mentioned, the behavior of the CH_2 group (C6 carbon), compared with other sugar carbons of **1**, is

dramatically different (the ^{13}C $T^*_{1\rho}$ of C6 is more than five times lower). In a first approximation it can be assumed that distinction is due to differences in the number of directly bonded protons [Eqn (2)]. More detailed discussion also requires consideration of the distinction of the $M^{(2)}_{C-H}$ parameter [Eqn (5)]. The bonded proton contribution dominates $M^{(2)}_{C-H}$ and bonded C—H dipolar interactions are identical. In general, in the case when τ_D is the same for both CH and CH_2 carbons, the difference in T^D_{CH} values arises from the ca two times larger value of $M^{(2)}_{C-H}$ for CH_2 carbons. From our results, it is apparent that the distinction of ^{13}C $T_{1\rho}$ for **1** is larger than expected. Hence it can be assumed that the correlation times for spin fluctuations of the CH_2 carbon compared with other sugar ring carbons of **1** are different owing to the contribution of the $T^C_{1\rho}$ pathway and distinction of internal dynamics.

Comparative analysis of **1** and **2** is an additional source of information about the molecular motion of both compounds. In general the ^{13}C $T_{1\rho}$ values for **2** are considerably larger (see Table 4), but the trend showing that the relaxation time of C6 is shorter than those of other sugar carbons is preserved. It is worth noting that the C3 and C4 carbons, split by an oxygen atom in a three-membered ring, have relatively long $T^*_{1\rho}$ and the distinction between the C1–C5 carbons is larger as in **1**.

As expected, the differences between ^{13}C $T^*_{1\rho}$ of aromatic signals are significant. The quaternary carbons C7 and C10 show very slow decay although the difference between the relaxation rates is apparent. The methine CH carbons (C8 and C9) relax much faster and the ^{13}C $T_{1\rho}$ values are comparable to those for C1–C5 sugar carbons. Finally, it is worth stressing that the relaxation times of the aromatic group of **1** are significantly shorter than those of **2** and this observation is consistent with data obtained for sugar residues.

The methyl carbon $T^*_{1\rho}$ data do not follow an exponential dependence on B_1 and are even independent of the rotating field at 36.7 kHz and higher values. This behavior is consistent with the motional pathway $T^C_{1\rho}$ dominating at high fields and with increasing contribution of the spin–spin pathway at lower rotating-frame fields.

DISCUSSION

In this project we characterized two models with a well-defined x-ray structure.[16] Both compounds crystallize in the $P2_12_12_1$ space group, orthorhombic system and four molecules in the unit cell. Despite the opposite orientation of the oxirane and thiirane groups, the overall conformations of the five- and six-membered rings remain the same. The *p*-tolylsulfonyl group is nearly synclinal with respect to the thiirane ring (**1**) and antiperiplanar with respect to the oxirane ring (**2**). As we found, such an arrangement has a significant influence on molecular packing. Figure 7 shows the unit cells for both compounds. Compound **2** is more tightly packed (the density of crystals is 1.464 g cm^{-3} for **1** and 1.495 g cm^{-3} for **2**).

Both compounds are involved in a number of C—H···O hydrogen bonds. A search of the *x*-ray data revealed that in case of **2** there are two intermolecular interactions with a contribution of the sulfonyl group. Owing to hydrogen bonding between C6-H and oxygen (H···O distance 2.487 Å, C—H···O angle 133.99°) and C11-H and the oxygen of the sulfonyl group of the neighboring group (H···O distance 2.561 Å, C—H···O

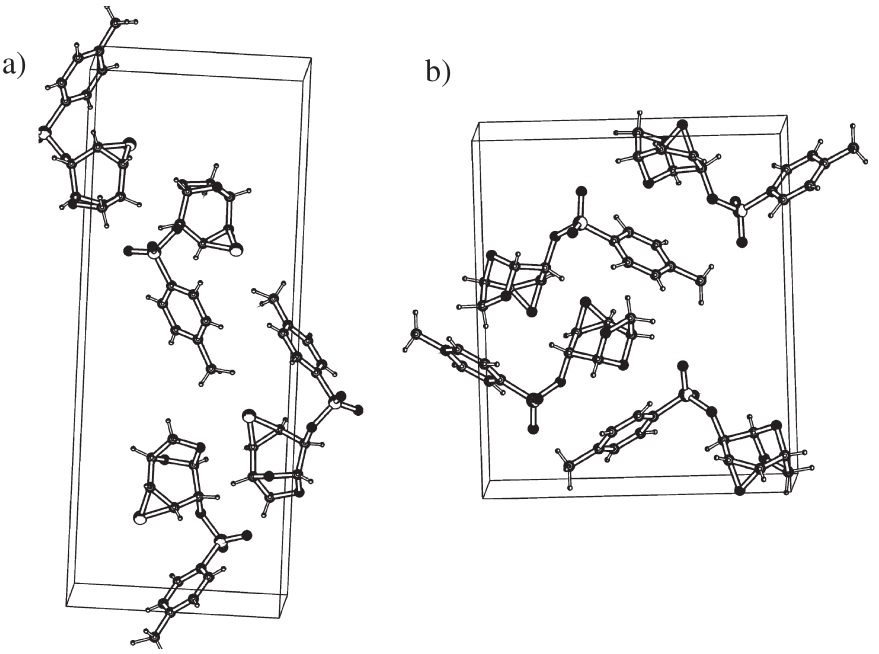

Figure 7. Molecular packing in the unit cell of (a) **1** and (b) **2**

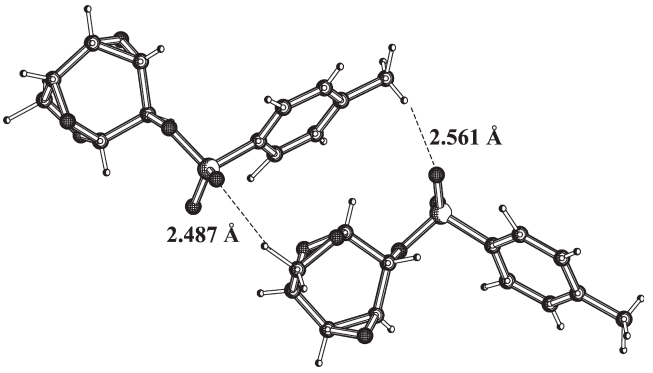

Figure 8. C—H···O intermolecular interactions in head-to-tail dimer of **2**

angle 164.30°), these two molecules form dimers in a head-to-tail orientation (Fig. 8). There are also strong interactions between the C2-H proton and O3 oxygen of the oxirane ring (H···O distance 2.358 Å, C—H···O angle 133.99°) and between the C4-H proton and O5 oxygen of the pyranose ring (H···O distance 2.387 Å, C—H···O angle 144.71°).[16]

The x-ray data for **1** showed three C—H···O intermolecular contacts (weaker than in **2**) and one C—H···S interaction. As found, the hydrogen on the C6 carbon is involved in interaction with the O1 oxygen (H···O distance 2.577 Å, C—H···O angle 160.75°), and the hydrogen on C2 is in contact with the oxygen of the sulfonyl group (H···O distance 2.697 Å, C—H···O angle 133.90°). Finally, the C11 methyl group is involved in interaction with the sulfur of the thiirane ring (H···S distance 2.845 Å, C—H···S angle 136.34°).[16]

Comparing the relaxation times in the rotating frame at $B_1 = 36.7$ kHz for **1** and **2**, we assume that the distinction of ^{13}C $T^*_{1\rho}$ is due to the difference in intramolecular dynamics related to the molecular structure (thiirane, oxirane ring) and difference in strength of C—H···O intermolecular interactions. A typical $T_{1\rho}$ curve has a minimum in its relaxation time vs correlation time plot. The slow side of the curve can be interpreted in such a way that a decrease in $T_{1\rho}$ indicates increased molecular motion, whereas the fast side of the curve can be interpreted in such a way that a decrease in $T_{1\rho}$ indicates decreased molecular motion. The relaxation of all carbons for **1** and **2** indicates motions on the slow side of the $T_{1\rho}$ minimum. The general trend that for the more rigid lattice of **2** all carbons are characterized by longer ^{13}C $T_{1\rho}$ (slower motion) is apparent from Table 4. For both samples, the ^{13}C $T_{1\rho}$ of C6 carbons is significantly shorter than others. Keeping in mind the discussion in the previous section, we postulate that the five-membered pyranose ring is more flexible than the residual part of sugar rings. Moreover, the ratio of the average value of $T^*_{1\rho}$ for C1–C5 atoms versus $T_{1\rho}$ of C6 is 5.8 for **1** and 3.8 for **2**. This means that for the latter compound relative motion of C6 is slower, very likely because of a significant contribution of C—H···O interaction. For **2**, the ^{13}C $T_{1\rho}$ values for C3 and C4 carbons are considerably longer. From XRD data, it is apparent that the C3—C4 bond distance is much shorter (1.446 Å) than the corresponding bond of thiirane (1.481 Å). It can be suggested that for **2** this part of the sugar molecule is more rigid than other atoms.

Replacing sulfur by oxygen has an influence on the values of the ^{13}C shielding parameters and orientation of principal elements of the chemical shift tensor with respect to the molecular frame. It is worth noting that the span Ω parameter, which reflects the distortion from tetrahedral geometry, is significantly larger for the C3 and C4 carbons of **2** which is consistent with the XRD data. This distinction is not so evident for **1**, very likely for the reason discussed above. Moreover, the skew parameter κ, which reflects the distribution of electron density for a particular center for those sugar carbons which are involved in the formation of hindered rings (C1, C3, C4), has negative values. The lowest values were found for the C3 and C4 carbons of the oxirane ring, which is consistent with the relationship between NMR spectral parameters and molecular structure.

CONCLUSIONS

Weak intra- and intermolecular interactions have great importance in crystal engineering, supramolecular chemistry and molecular recognition.[35] In this work, we considered the correlation between solid-state NMR spectral parameters and the molecular packing of samples with different strengths of C—H···O contacts. Our results show that analysis of dynamic processes on the kilohertz scale is a sensitive tool, which allows more tightly packed systems to be recognized. Inspection of ^{13}C $T_{1\rho}$ relaxation times for individual carbon atoms provides the 'bridge' between internal motion and intermolecular contacts. Finally, it is worth noting that even very rigid carbohydrate derivatives can undergo dynamic processes in the solid state, although the scale of the molecular motions has to be verifying by spectroscopic techniques.

EXPERIMENTAL

Compounds **1** and **2** were obtained as described in the literature.[16] ^{13}C CP/MAS spectra were recorded employing a Bruker DSX 300 instrument, with a 3 ms contact time, repetition delay 20 s and spectral width 25k Hz. The sample was spun at 1 and 7 kHz; 2K data point FIDs were accumulated. Data were processed off-line using the WIN-NMR program running on a PC.[36] Glycine was used for the setting the Hartman–Hahn condition for CP/MAS and adamantane as a secondary chemical shift reference $\delta = 38.48$ and 29.46 ppm from external

TMS.[37] The principal components δ_{ii} are defined as $\delta_{11} > \delta_{22} > \delta_{33}$. From δ_i values, the shielding parameters, anisotropy $\Delta\delta$, asymmetry η, span Ω and skew κ, were calculated.[38] The ^{13}C T_1 and ^{13}C $T_{1\rho}$ measurements were performed with the same spectral parameters as were used for CP/MAS experiments. The sample was spun at 7 kHz and the standard pulse sequences were used. Twelve FIDs, 100 scans each, were recorded with recovery delay 600 s for T_1 and 20 s for $T_{1\rho}$.

A sample spinning speed of 1 kHz was used in PASS-2D experiments. The 16-point experiment t_1 data were replicated to 256 points. One-dimensional CSA spinning sidebands was obtained from t_1 slices taken at isotropic chemical shifts in the ω_2 dimension of the 2D spectrum. The magnitudes of the principal elements of the CSA were obtained from the best-fitting simulated spinning patterns. Simulations of the spinning CSA sidebands spectra were carried out on a PC using the SIMPSON program under a LINUX environment.

DFT GIAO calculations were carried out with the Gaussian 98 program running on a Silicon Graphics Power Challenge computer. The GIAO method with the B3PW91 hybrid method and 6–311++G** basis set was used to calculate NMR parameters. The orientation of principal elements of chemical shift tensors with respect to the molecular frame of **1** and **2** were derived by means of theoretical approach employing standard procedure described in the Gaussian manual.

Acknowledgment

The authors are grateful to Professor Maria Michalska for the generous gift of compounds **1** and **2**.

REFERENCES

1. Peters T, Pinto BM. *Curr. Opin. Struct. Biol.* 1996; **6**: 710–720.
2. Van Halbeek H. In *Encyclopedia of Nuclear Magnetic Resonance*, Grant DM, Harris RK (eds). Wiley: Chichester, 1996; 1107–1137.
3. Rao BDN, Kemple MD (eds). *NMR as a Structural Tool for Macromolecules: Current Status and Future Directions.* Plenum Press: New York, 1996.
4. Duss JØ, Gotfredsen ChH, Bock K. *Chem. Rev.* 2000; **100**: 4589–4614.
5. Weller ChT. In *Encyclopedia of Spectroscopy and Spectrometry*, Lindon JC (ed). Academic Press: San Diego, 2000; 172–180.
6. Palmer G III, Williams J, McDermott A. *J. Phys. Chem.* 1996; **100**: 13293–13310.
7. Dais P. *Adv. Carbohydr. Chem. Biochem.* 1995; **51**: 63.
8. Kjellberg A, Rundlöf T, Kowalewski J, Widmalm G. *J. Phys. Chem. B* 1998; **102**: 1013.
9. (a) Saito H. In *Encyclopedia of Nuclear Magnetic Resonance*, Grant DM, Harris RK (eds). Wiley: Chichester, 1996; 3740–3745; (b) Potrzebowski MJ. *New Advanced in Analytical Chemistry*, Rahman A-U (ed). Harwood Publishers: Amsterdam: The Netherlands, 2000; 359–404, and references cited therein.
10. Voelter W, Khan KM, Shekhani MS. *Pure Appl. Chem.* 1996; **68**: 1347–1353.
11. Izquiderdo I, Plaza T, Asenjo R, Ramirez A. *Tetrahedron: Asymmetry* 2002; **13**: 1417–1421.
12. Dais P. *Carbohydr. Res.* 1994; **263**: 13–24.
13. Maeler L, Wildmalm G, Kowalewski J. *J. Phys. Chem.* 1996; **100**: 17103–17110.
14. Krivdin LB, Sauer SPA, Peralta JE, Contreras RH. *Magn. Reson. Chem.* 2002; **40**: 187–194.
15. Wang AL, Lu S-J, Fu H-X, Wang H-Q, Huang X-Y. *Carbohydr. Res.* 1996; **281**: 301–305.
16. Michalska M, Kudelska W, Pluskowski J, Koziol AE, Lis T. *J. Chem. Soc., Perkin Trans 1* 1994; 979–983.
17. Potrzebowski MJ, Kaźmierski S, Michalska M, Olejniczak S, Ciesielski W, Latanowicz L. *J. Mol. Struct.* 2001; **597**: 7–19.
18. Kaźmierski S, Olejniczak S, Potrzebowski MJ. *Solid State Nucl. Magn. Reson.* 2000; **16**: 131–139.
19. Metz G, Wu X, Smith SO. *J. Magn. Reson. A* 1994; **110**: 219–227.
20. Bennett AE, Rienstra CM, Auger M, Lakshmi KV, Griffin RG. *J. Chem. Phys* 1995; **103**: 6551–6958.
21. (a) Hu J, Wang W, Liu F, Solum MS, Alderman DW, Pugmire RJ. *J. Magn. Reson. A* 1995; **113**: 210–222; (b) Alderman DW, McGeorge G, Hu JZ, Pugmire RJ, Grant DM. *Mol. Phys.* 1998; **95**: 1113; (c) Frydman L, Chingas GC, Lee YK, Grandinetti PJ, Eastman MA, Barral GA, Pines A. *J. Chem. Phys.* 1992; **97**: 480; (d) Kolbert AC, Griffin RG. *Chem. Phys. Lett.* 1990; **166**: 87–91.
22. Antzutkin ON. *Prog. Nucl. Magn. Reson. Spectrosc.* 1999; **35**: 203–226.
23. Antzutkin ON, Shekar SC, Levitt MH. *J. Magn. Reson. A* 1995; **115**: 7–19.
24. Dixon WT. *J. Chem. Phys.* 1982; **77**: 1800–1809.
25. Bak M, Rasmussen JT, Nielsen NC. *J. Magn. Reson.* 2000; **147**: 296–330.
26. Grant DM, Facelli JC, Alderman DW, Sherwood MH. In *Nuclear Magnetic Shielding and Molecular Structure*, Tossell JA (ed). Kluwer: Dordrecht, 1993; 367–384.
27. Malkin VG, Malkina OL, Eriksson LA, Salahub DR. In *Theoretical and Computational Chemistry*, vol. 2, Seminaro JM, Politzer P (eds). Elsevier: Amsterdam, 1995.
28. Frisch MJ, Trucks GW, Schlegel HB, Scuseria GE, Robb MA, Cheeseman JR, Zakrzewski VG, Montgomery JA Jr, Stratmann RE, Burant JC, Dapprich S, Millam JM, Daniels AD, Kudin KN, Strain MC, Farkas O, Tomasi J, Barone V, Cossi M, Cammi R, Mennucci B, Pomelli C, Adamo C, Clifford S, Ochterski J, Petersson GA, Ayala PY, Cui Q, Morokuma K, Salvador P, Dannenberg JJ, Malick DK, Rabuck AD, Raghavachari K, Foresman JB, Cioslowski J, Ortiz JV, Baboul AG, Stefanov BB, Liu G, Liashenko A, Piskorz P, Komaromi I, Gomperts R, Martin RL, Fox DJ, Keith T, Al-Laham MA, Peng CY, Nanayakkara A, Challacombe M, Gill PMW, Johnson B, Chen W, Wong MW, Andres JL, Gonzalez C, Head-Gordon M, Replogle ES, Pople JA. *Gaussian 98, Revision A.6*. Gaussian: Pittsburgh, PA, 1998.
29. Liu F, Phung DW, Alderman DW, Grant DM. *J. Am. Chem. Soc.* 1996; **118**: 10629–10634.
30. Sastry DL, Takegoshi K, McDowell CA. *Carbohydr. Res.* 1987; **165**: 161–171.
31. Lyerla JR. In *Methods in Stereochemical Analysis, High Resolution NMR Spectroscopy of Synthetic Polymers in Bulk*, vol. 7, Komoroski RA (ed). VCH: Deerfield Beach, FL, 1986; 63–120.
32. Torchia DA. *J. Magn. Reson.* 1978; **30**: 613–616.
33. VanderHart DL, Garroway AN. *J. Chem. Phys.* 1979; **71**: 2773–2787.
34. Garroway AN. *J. Magn. Reson.* 1979; **34**: 283–293.
35. Desiraju GR. *Acc. Chem. Res*. 2002; **35**: 565–573, and references cited therein.
36. *WIN-NMR vereion 6.0*. Bruker-Franzen Analytik: Karlsruhe 1996.01.01.
37. Morcombe CR, Zilm KW. *J. Magn. Reson*. 2003; **162**: 479–486.
38. Mason I. *Solid State NMR* 1993; **2**: 285–288.